Biosensors and Bioelectronics 190 (2021) 113264

Contents lists available at ScienceDirect

Biosensors and Bioelectronics

journal homepage: www.elsevier.com/locate/bios

A microfluidic field-effect transistor biosensor with rolled-up indium nitride microtubes

Pengfei Song [a,b,c], Hao Fu [a,b], Yongjie Wang [d], Cheng Chen [e], Pengfei Ou [f], Roksana Tonny Rashid [g], Sixuan Duan [c], Jun Song [f], Zetian Mi [g,h], Xinyu Liu [a,*]

[a] Department of Mechanical and Industrial Engineering, University of Toronto, 5 King's College Road, Toronto, Ontario, M5S 3G8, Canada
[b] Department of Mechanical Engineering, McGill University, 817 Sherbrooke Street West, Montreal, Quebec, H3A 0C3, Canada
[c] School of Advanced Technology, Xi'an Jiaotong-Liverpool University, 111 Ren'ai Road, Suzhou, 215000, China
[d] School of Science, Harbin Institute of Technology-Shenzhen, 1 Pingshan Road, Shenzhen, 518000, China
[e] School of Aeronautics, Northwestern Polytechnical University, 1 Dongxiang Road, Xi'an, 710000, China
[f] Department of Mining and Materials Engineering, McGill University, 3610 Rue University, Montreal, Quebec, H3A 0C5, Canada
[g] Department of Electrical and Computer Engineering, McGill University, Montreal, Quebec, H3A 0E9, Canada
[h] Department Electrical Engineering and Computer Science, University of Michigan, Ann Arbor, MI, 48109, USA

ARTICLE INFO

Keywords:
Biosensor
Rolled-up microtube
Field-effect transistor
Indium nitride
Disease diagnostics

ABSTRACT

Field-effect-transistor (FET) biosensors capable of rapidly detecting disease-relevant biomarkers have long been considered as a promising tool for point-of-care (POC) diagnosis. Rolled-up nanotechnology, as a batch fabrication strategy for generating three-dimensional (3D) microtubes, has been demonstrated to possess unique advantages for constructing FET biosensors. In this paper, we report a new approach combining the two fascinating technologies, the FET biosensor and the rolled-up microtube, to develop a microfluidic diagnostic biosensor. We integrated an excellent biosensing III-nitride material—indium nitride (InN)—into a rolled-up microtube and used it as the FET channel. The InN possesses strong, intrinsic, and stable electron accumulation ($\sim 10^{13}$ cm^{-2}) on its surface, thereby providing a high device sensitivity. Multiple rolled-up InN microtube FET biosensors fabricated on the same substrate were integrated with a microfluidic channel for convenient fluids handling, and shared the same external electrode (inserted into the microchannel outlet) for gating voltage modulation. Using human immunodeficiency virus (HIV) antibody as a model disease marker, we characterized the analytical performance of the developed biosensor and achieved a limit of detection (LOD) of 2.5 pM for serum samples spiked with HIV gp41 antibodies. The rolled-up InN microtube FET biosensor represents a new type of III-nitride-based FET biosensor and holds significant potential for practical POC diagnosis.

1. Introduction

Miniaturized and sensitive biosensors capable of rapidly detecting disease-relevant biomarkers at the point of care (POC) have enormous impact on healthcare by enabling early-stage disease diagnosis and timely treatment (Yager et al., 2008). Conventional diagnostic tests are performed in clinical laboratories, and may take long turnaround time (hours and even days) for potential patients to get the results. This may cause delayed treatment and impose unnecessary anxieties/stresses on the patients. For patients carrying infectious diseases, the long waiting time before determinative diagnosis may lead to further spreading of the diseases due to the patients' unawareness of their conditions (Gubbins et al., 2014; Qin et al., 2020). POC devices offer an excellent solution for providing accurate, quality-assured tests near patients in a rapid fashion (e.g., in minutes), and can expedite diagnosis and treatment initiation in under-served regions/communities and/or in resource-poor settings (Fu et al., 2019; Pant Pai, 2007; Vickerman et al., 2006; Zhao and Liu, 2016).

There has been a significant technological trend of developing POC devices to meet the urgent demands for timely and sensitive diagnostic services. With many apparent advantages suitable for POC applications, FET biosensors have emerged as an enabling platform technology for developing sensitive and rapid POC tests (Kwon et al., 2012; Shoorideh and Chui, 2014). FET biosensors usually feature fast response, label-free assay, high sensitivity (enabled by the high sensitivity of the FET channel material to surface binding of molecules), good compatibility with batch fabrication, and thus low unit cost (Cui et al., 2001;

* Corresponding author.
E-mail address: xyliu@mie.utoronto.ca (X. Liu).

https://doi.org/10.1016/j.bios.2021.113264
Received 20 January 2021; Received in revised form 15 April 2021; Accepted 16 April 2021
Available online 1 May 2021

Kauffman and Star, 2008). The miniature nature of FET biosensors also permits their easy integration into microfluidic devices to gain additional advantages such as multiplexed testing (detection of multiple markers) and less sample/reagent consumption (Ang et al., 2011; Xu et al., 2014).

Rolled-up nanotechnology is a novel strategy combining bottom-up thin-film growth/deposition and top-down lithography for fabricating three-dimensional (3D) tubular micro/nano-structures, which have shown unique advantages for developing microfluidic biosensors. First, the rolled-up microtubular structure has a small footprint and can be batch-fabricated and integrated into microfluidic channels for convenient fluid handling and multiplexed detection. The rolled-up microtube itself also naturally forms a microfluidic channel that can transport fluids for biosensing. The first rolled-up microtube fluidic sensor was reported in 2008 (Bernardi et al., 2008). After that, rolled-up microtubes have been used to develop a variety of biosensors based on different sensing mechanisms, including optical ring resonator (Huang et al., 2010; Li et al., 2019; Song et al., 2018; Wang et al., 2019; Zhao et al., 2012), Raman spectroscopy (Yin et al., 2012; Zhang et al., 2015), electrical sensing (Egunov et al., 2021; Grimm et al., 2013), magnetic sensing (Karnaushenko et al., 2018; Mö;nch et al., 2011), and self-propelled micromotor-based sensing (Han et al., 2016), to name a few. Second, the exceptional fabrication flexibility of rolled-up nanotechnology allows microtubes to be made from a variety of functional materials including semiconductor thin-films and thus serve as FET channel structures, promising enhanced performance from the semiconductor microtube-based FET biosensors (Li and Mi, 2009; Li, 2011; Mei et al., 2008). Last, using a tubular structure as the FET channel has been demonstrated to enhance the sensitivity of the FET biosensor, by reducing the Debye screening effect (Shoorideh and Chui, 2014). Because of the Debye screening existing on its channel surface, an FET biosensor is only responsive to the charged molecules within a certain length (the Debye length), and the device sensitivity is thereby severely limited (Stern et al., 2007).

This work aims to take full advantage of this merit to fabricate rolled-up indium nitride (InN) microtubes and use them to construct a new type of FET biosensor. Although various materials including 2D materials (Cui et al., 2018; Xu et al., 2017; Zhou et al., 2019), III-V group materials (Dastjerdi et al., 2015; Mei et al., 2009; Yu et al., 2015), and polymers (Hu et al., 2018; Jager et al., 2000; Zakharchenko et al., 2011) have been used to construct rolled-up microtubes, the semiconductive InN material has not been explored. InN nanostructures possess the highest intrinsic surface electron accumulation ($\sim 10^{13}$ cm^{-2}) among all III-nitride materials, and this inherent property of InN cannot be easily altered physically or chemically during microfabrication (Lu et al., 2004; Naoi et al., 2007). The high surface electron accumulation makes it highly sensitive to the binding of charged biomolecules, and thus ideal for serving as the channel structure of an FET biosensor (Chen et al., 2006; Lu et al., 2003; Mahboob et al., 2004). There has been only one attempt to develop microtube-based FET chemical sensors (Grimm et al., 2013). Grimm et al. developed the first rolled-up microtube FET (RUM-FET) biosensor using InGaAs/GaAs bilayers. This work only demonstrated the sensing capability of the RUM-FET using different solvents, and the detection of real disease markers was not demonstrated. In addition, the semiconductor materials used in the design of Grimm et al., InGaAs and GaAs, have lower surface electron accumulation densities than InN.

In this paper, we report a new type of FET biosensor integrating high-performance InN tubular microstructures, and demonstrate label-free detection of human immunodeficiency virus (HIV) antibodies. The InN thin films were deposited, through facile direct-current (DC) reactive sputtering, on a bilayer of strain-engineered SiO_x/SiN_x (bottom/top) nanomembranes, which served as the rolling vehicle to form SiO_x/SiN_x/InN microtubes. The material properties of the deposited InN were characterized using X-ray photoelectron spectroscopy (XPS) and scanning electron microscopy (SEM). The InN microtube was functionalized with capture proteins specific to the HIV antibodies using convenient (3-Aminopropyl) trimethoxysilane as the chemical linker, and the surface chemistries were characterized by XPS (Chen et al., 2006). Using the InN RUM-FET biosensor, we performed label-free detection of HIV gp41 antibodies, and achieve a limit of detection of 0.1 ng mL^{-1}.

2. Materials and methods

2.1. Materials and reagents

All chemicals used in the experiments, including (3-Aminopropyl)-trimethoxysilane (APTMS) (97%), 2.5% (v/v) glutaraldehyde (GA), 1 × phosphate buffered saline (PBS), and 0.1% bovine serum albumin (BSA), were purchased from Sigma-Aldrich (Oakville, Canada). HIV pg41 antibody was purchased from ViroGen.

2.2. Design of rolled-up InN microtubes

As shown in Fig. 1a, the rolled-up microtubes were formed from three layers of SiO_x/SiN_x/InN nanomembranes (bottom to top). The bottom two layers of SiO_x/SiN_x, which are much thicker than the top InN layer (15 nm/50 nm vs. 5 nm), were deposited with controlled built-in stresses using plasma enhanced chemical vapor deposition (PECVD) and served as the driver for microtube self-rolling upon release from the substrate. The thicknesses of the bottom two layers heavily affect the yield of the rolling-up process, as different thickness combinations lead to different strain gradient in the bottom two layers. We experimentally demonstrated that the combination of 15 nm SiO_x and 50 nm SiN_x yielded the best fabrication yield (Song et al., 2018). The InN film was set to be only 5 nm thick for two reasons. First, a thick InN layer could jeopardize the microtube self-rolling process by affecting the strain gradient, preventing the SiO_x/SiN_x/InN nanomembranes from completely rolling up due to a large external strain gradient posed by the thick InN layer. Second, a thick sputtering-deposited InN film could be difficult to be patterned through the lift-off technique (see the "Fabrication of the rolled-up InN microtubes" section), as the edge of the sacrificial photoresist under the InN film will be also coated by the thick InN film. Once a SiO_x/SiN_x/InN microtube is rolled up, the thin layer of InN will be exposed on the inner wall of the microtube (Fig. 1a), serving as the biosensing surface. The length of the microtube is 350 μm with a diameter of ~20 μm, and the microtubes in the same row are 650 μm away from each other. The FET channel length (the gap between the two electrodes) was designed to be short (20 μm) to enhance the FET sensing performance. The major design parameters of the FET were determined by considering the microfabrication resolution, the arrangement of microtube arrays on the silicon wafer, and the general FET design rules for increasing the biosensing performance. For instance, reducing the FET channel length could improve the device sensitivity but may increase the fabrication difficulty and thus sacrifise the fabrication yield (Fathil et al., 2018)."

The InN inner wall of the microtube forms an ideal concave surface contacting with the analyte solution, and this configuration has been theoretically determined to reduce the electrostatic screening on the biosensing surface and thus prove the device's sensitivity of charge detection in electrolytic environments (Shoorideh and Chui, 2014). The micrometer size and batch fabrication process of the rolled-up InN microtube also allow the integration of multiple InN RUM-FETs inside a microfluidic channel to facilitate the solution delivery and reduce the sample/reagent consumptions. As shown in Fig. 1c, we batch-fabricated two rows of InN RUM-FET biosensors (six in each) on the same silicon (Si) substrate, and enclosed each row of the biosensor in a separate PDMS microfluidic channel. When running a test, the sample solution was delivered into each microchannel via its inlet, and a miniaturized Ag/AgCl electrode (ET073-1, eDAQ) was inserted into the microchannel outlet to modulate the FET's gating voltage (Fig. 1d). A previous study has shown that the use of a single miniaturized gate electrode for

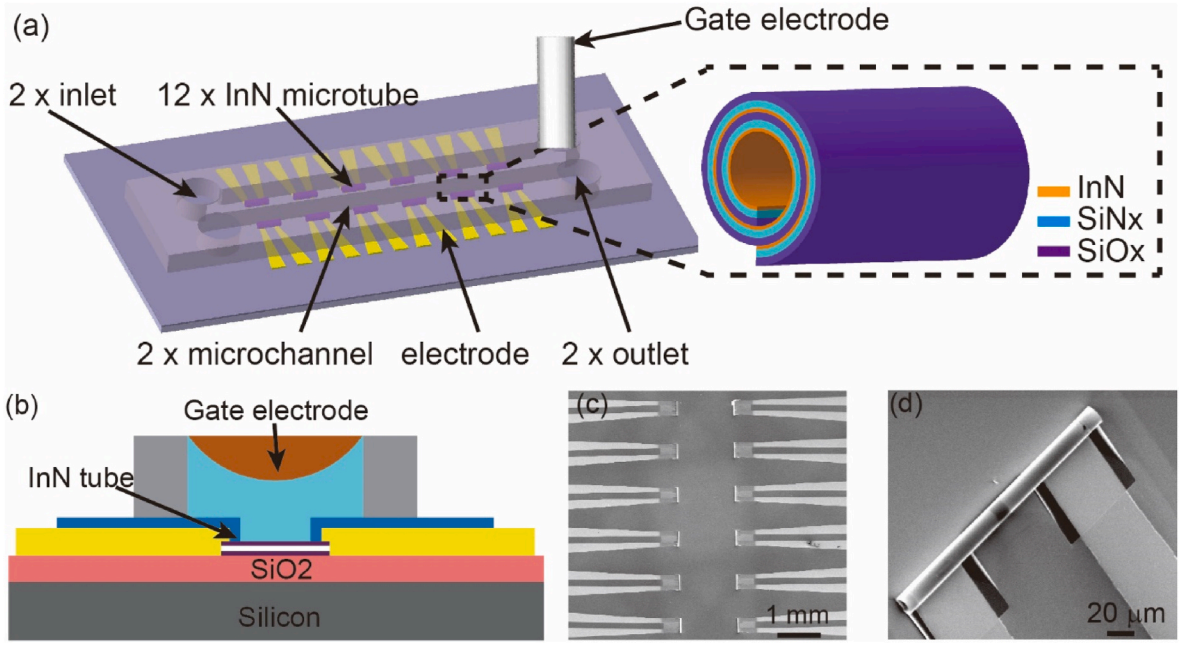

Fig. 1. Design of the InN RUM-FET biosensor. (a) Schematics of 12 InN RUM-FET biosensors enclosed in two microfluidic channels. The channel width is 400 μm and length is 6.5 mm, which are large enough to accommodate 12 InN microtubes. The zoomed-in view shows the three-layer structure of the InN microtube. (b) Schematic of the experiment condition with an gate electrode inserted into the channel outlet. (c) SEM photograph of an array of 12 fabricated InN microtubes. (d) A high-magnification SEM photograph of an InN microtube.

multiple FETs does not cause performance inconsistency of the FETs (Xu et al., 2014). The diameter of the gate electrode is 2 mm, which is slightly larger than that of the outlet diameter (1.5 mm) of the microfluidic device. Therefore, once inserted into the device outlet, the electrode formed a stable mechanical and electrical connection.

2.3. Fabrication of rolled-up InN microtubes

The rolled-up microtubes were fabricated through controlled release of strain-engineered SiO_x/SiN_x/InN thin-films. This fabrication process was adapted from a previous protocol we reported for fabricating SiO_x/SiN_x microtubes (Song et al., 2018). As shown in Fig. 2, the process started from electron-beam deposition (BJD, 1800; Temescal) of an aluminum sacrificial layer (50 nm) on a cleaned Si wafer (Fig. 2a), followed by PECVD deposition (Oxford Plasma 100) of SiO_x/SiN_x (bottom/top) thin films (Fig. 2b). The PECVD parameters of 8.5 sccm SiH_4 with 710 sccm N_2O, and 10 sccm SiH_4 with 10 sccm NH_3 were experimentally determined to produce suitable film stresses for SiO_x (-831.5 ± 21.4 MPa, n = 5) and SiN_x (221.5 ± 12.1 MPa, n = 5), respectively. The deposition temperature, power, and working frequency were 300 °C, 70 W, and 13.56 MHz for both layers. The SiO_x/SiN_x bilayer acts as the rolling vehicle to roll-up the subsequently deposited InN thin film. Then, the SiO_x/SiN_x bilayer was patterned into a U-shape through standard photolithography (photoresist: S1813, MicroChem) and wet etching by 10:1 diluted hydrofluoric acid.

Once the U-shaped SiO_x/SiN_x was formed, InN thin film was deposited and patterned into the same U-shape, and was precisely aligned on the top of the SiN_x/SiO_x bilayers (Fig. 2c). The 5 nm InN thin film was deposited by DC reactive sputtering (E14, Denton). Briefly, the pure indium target (99.999%) was used under an argon and nitrogen gas environment (Ar 20 sccm, and N_2 100 sccm). The DC current was set to 0.22 A and substrate temperature was maintained at 45 °C. After the

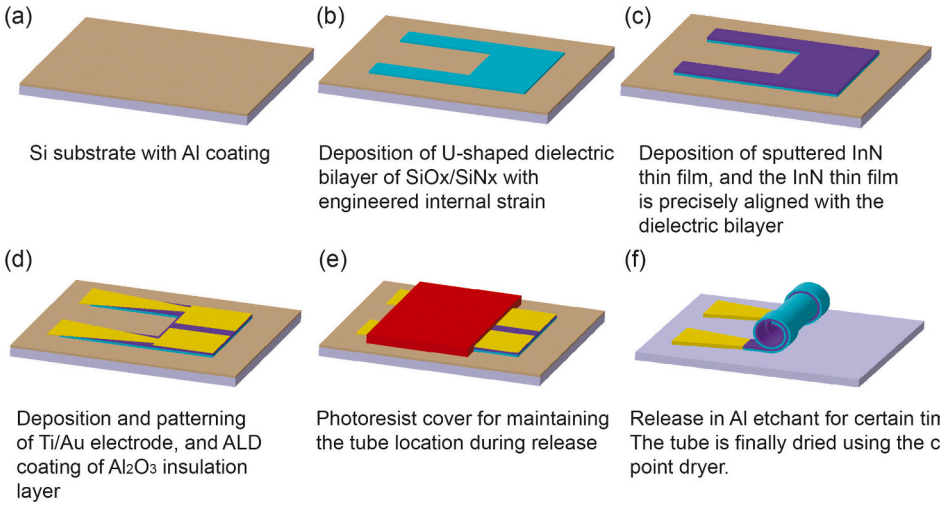

Fig. 2. Fabrication process of the rolled-up InN microtube. (a) The pre-cleaned silicon wafer was coated with 50 nm Al sacrificial layer. (b) The strain-engineered SiO_x/SiN_x bilayer was deposited by PECVD and patterned by wet etching. (c) The InN thin film was then deposited by sputtering and patterned by lift-off. (d) Another lift-off was performed for pattering the e-beam deposited Ti/Au electrode. The atomic-layer-deposition (ALD) coating of Al_2O_3 was also performed to cover the electrode surface for preventing the direct solution contact with the electrode. (e) Photoresist cover was used for maintaining the tube location during the release. (f) The tube was finally released from the substrate using the Al etchant and dried in a critical point dryer. (For interpretation of the references to color in this figure legend, the reader is referred to the Web version of this article.)

growth time of 120 s, one lift-off process was performed using the S1813 photoresist (MICROPOSIT) and the 1165 solution (65 °C for at least 30 min). Two gold electrodes were then fabricated on top of the InN layer by performing another lift-off of the e-beam (BJD, 1800; Temescal) deposited biolayer of titanium/gold (5 nm/15 nm), leaving a 20 μm gap in between as the biosensing area of the FET channel. The titanium/gold electrode was used to form Ohimc contact with the InN layer according to the previous reports (Chang et al., 2010; Oseki et al., 2014). The atomic layer deposition (ALD; GEMStar-8™) was finally used to insulate the electrode to avoid any exposure to the analyte solution. Another photolithography was performed for patterning a rectangular photoresist (S1813, MICROPOSIT) structure covering the legs of the U-shapes, which acted as the anchor of the SiO_x/SiN_x/InN nanomembranes during the releasing/rolling-up process. The releasing process was performed using the aluminum etchant type A (Transene Inc.) under elevated temperature (80 °C) to allow the SiO_x/SiN_x/InN nanomembranes to self-rolling upon the removal of the aluminum layer. The sample was then immersed in deionized (DI) wafer for stopping the etching. A critical point dryer (CPD, Tousimis) was finally used to dry the rolled-up microtubes; otherwise, the large surface tension during the air-environment drying process could lead to the microtube collapse.

2.4. InN material characterization

We utilized a variety of tools to characterize the synthesized InN thin film, including X-Ray photoelectron spectroscopy (XPS, Thermo-Scientific *K*-Alpha) and scanning electron microscopy (F50, FEI). The high-resolution XPS spectra with an energy resolution smaller than 0.2 eV were collected using Al-Kα ($h\nu$ = 1486.6 eV) as the X-Ray beam source. All XPS spectra were corrected and aligned using C *1s* (284.8 eV) as the reference.

2.5. InN surface biofunctionalization and device packaging

We employed an organosilane-based surface functionalization process (Fig. 3) to covalently bind the capture proteins on the InN surface, which was adapted from a previously established method (Chen et al., 2006). Briefly, the rolled-up InN microtube was first treated and activated by oxygen plasma (DSB6000, NanoPlas) for 10 min at 10 W power and 0.6 mTorr pressure, during which the substrate was maintained at 25 °C. The plasma activation process led to a dense layer of hydroxyl groups (–OH) on the InN surface and the Si substrate. We then immediately bonded the pre-prepared DPMS layer, which includes two microchannels fabricated through soft lithography, on the Si substrate to cover each row of RUM-FETs with one microchannel. The (3-aminopropyl)-trimethoxysilane (APTMS, 97%) solution was then infused into the microchannel to bind with the InN surface through Si–O bonds (Fig. 3). After 30-min reaction, we thoroughly washed the rolled-up microtubes with ethanol to remove extra APTMS. The 2.5% (v/v) glutaraldehyde (GA) solution (10 mM) was then infused into the microchannel for reacting with the amine ($–NH_2$) groups of APTMS, and providing aldehyde (CHO-) groups for subsequent capture probe immobilization. The reaction of APTMS and GA was also incubated for 30 min. After the GA treatment, the rolled-up microtubes were thoroughly washed with DI water, and then treated with 10 μg mL^{-1} HIV gp41 antibody solution for 30 min at room temperature. In the end, 1 × PBS solution was used to wash off the unbound antibodies. To avoid non-specific binding, we also used 0.1% bovine serum albumin (BSA) solution to block the InN surface through 10-min incubation followed by thorough washing by 1 × PBS. All the aforementioned surface reaction steps were carried out at room temperature (21 °C).

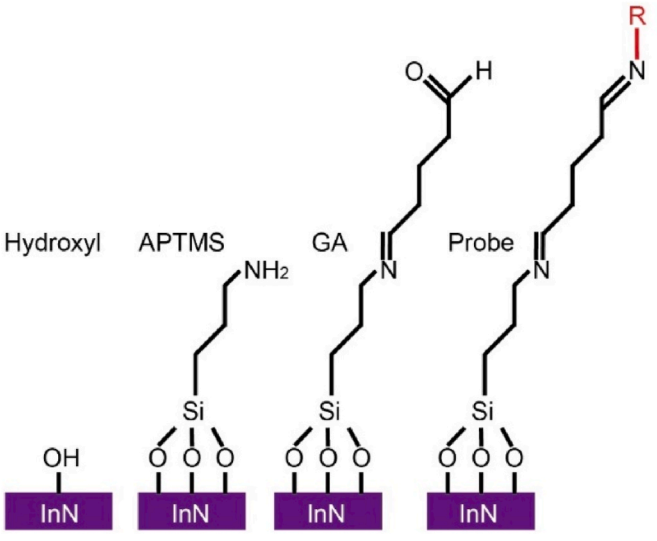

Fig. 3. Schematic diagram of the surface chemistry route for biofunctionalization of the InN thin film. The probe protein molecule in the final step is denoted as 'R'.

2.6. Device characterization

The electrical characteristics of the InN RUM-FET were measured by a precision dual-channel source meter (2602, Keithley). For measurements of the transport characteristics of the RUM-FET, the source-to-drain voltage (V_d) was set at 0.1 V and the solution gate voltage V_g was scanned from −0.5 V to 0.5 V. The sweep step of V_g was 100 mV, and for each step the applied V_g pulse was maintained for 2 s to stabilize the I_{ds} to ensure the reliability of the transport curve.

3. Results and discussion

3.1. Characterization of the InN thin film

Though molecular beam epitaxy (MBE) is widely used to produce high-quality InN thin films for device applications, the high temperature (550 °C) involved in the MBE growth could induce annealing effect on the strain-engineered SiO_x/SiN_x layers and thus release the built-in stresses of the nanomembranes. Therefore, it is not feasible to use the MBE method to integrate InN into the rolled-up microtubes. We adopted the DC reactive sputtering for growth of the InN thin film on the SiO_x/SiN_x bilayer, which is a low-temperature process and compatible with the fabrication of rolled-up microtubes (Lindgren et al., 2006). To verify the quality of the sputtered InN film, we first examined the chemical composition of the InN film by XPS. The XPS spectra, as shown in Fig. 4a and b, were collected from the InN thin film deposited on a SiN_x layer (to mimic the SiO_x/SiN_x bilayer). The In *3d* spectrum has two peaks at 443.8 eV and 451.4 eV (Fig. 4a), which are attributed to the doublet of In $3d_{5/2}$ and In $3d_{3/2}$, respectively. The N *1s* spectrum has one peak at 396.6 eV (Fig. 4b), corresponding to the nitrogen bonded with indium. The measured XPS spectra are in good agreement with previously reported data (Lindgren et al., 2002), confirming the successful growth of InN. Fig. 4c shows the SEM photograph of the 5 nm InN thin film deposited on the top of the SiN_x layer. It can be seen that the InN film shows continuous and highly uniform surface morphology.

3.2. Verification of the InN surface biofunctionalization

After successfully growth of the InN films, we experimentally verified the surface functionalization of the InN film with (3-aminopropyl)-trimethoxysilane (APTMS), which serves as the chemical linker for immobilizing capture proteins specific to the target protein marker (Chen et al., 2006; Li and Liu, 2016). XPS was used for probing the surface chemical change caused by surface chemical functionalization. For the InN film functionalized with APTMS, the bonding of APTMS molecules onto the plasma-treated InN surface was verified by

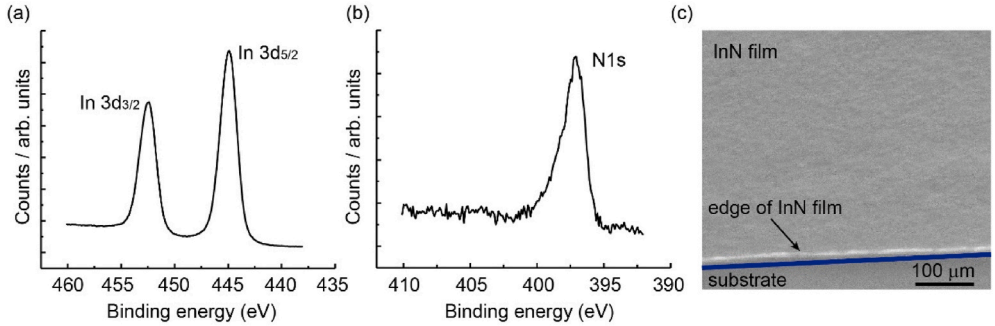

Fig. 4. Characterization of the sputtering-synthesized InN thin film. (a) In 3d core-level XPS spectra. (b) S 2p core-level XPS spectra. (c) SEM image of synthesized InN thin film.

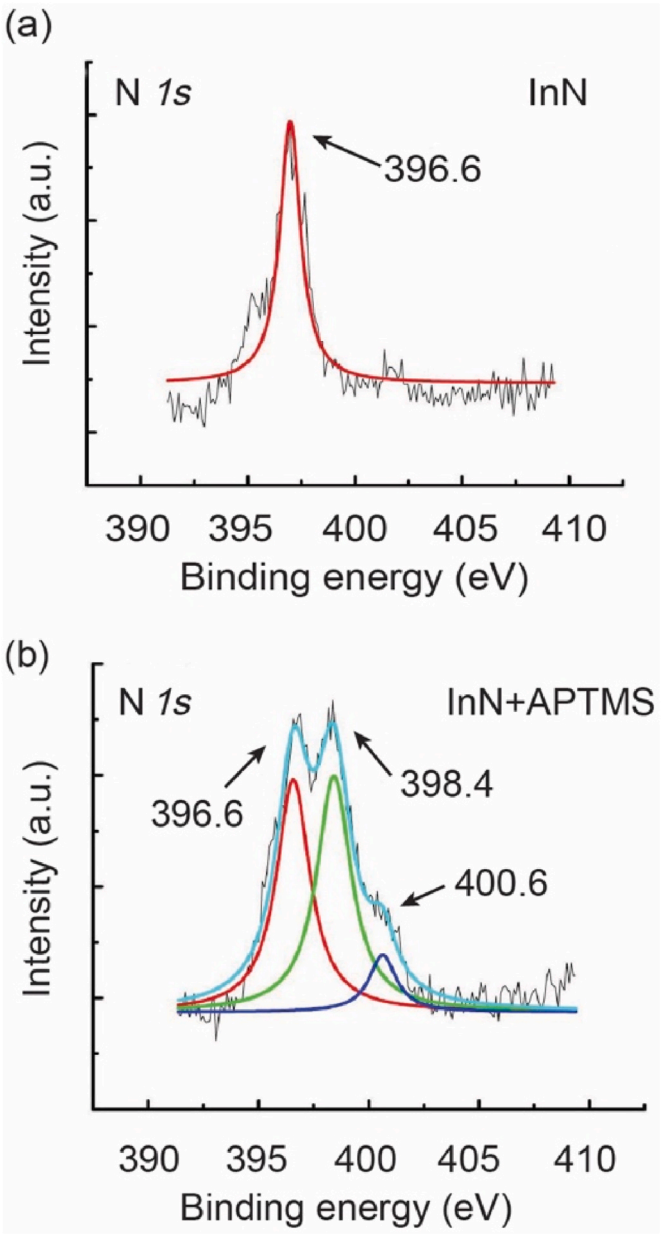

Fig. 5. N 1s core-level XPS spectra of (a) pristine and (b) APTMS-coupled InN thin films. The XPS spectra (black lines) are fitted to show the individual peaks (color lines). (For interpretation of the references to color in this figure legend, the reader is referred to the Web version of this article.)

observation of the XPS N *1s* spectra before and after the APTMS treatment (Chen et al., 2006). Fig. 5 shows the N *1s* core-level spectra unequivocally. Two new peaks at 398.4 eV and 400.6 eV were observed after the APTMS treatment (Fig. 5b). These two peaks correspond to the NH_2 and NH^{3+}, respectively, which are due to the immobilization of APTMS on the InN surface. For the pristine InN sample, only 396.6 eV peak was detected (Fig. 5a). These observations well agree with the previously reported results (Chen et al., 2006), suggesting that our APTMS-based surface functionalization is effective.

3.3. Electrical characterization of the InN RUM-FET

We first characterized the electrical properties of the fabricated InN RUM-FET. The device's conducting and transporting properties after biofunctionalization were measured, as shown in Fig. 6a and b. It can be seen from Fig. 6a that source-to-drain current increases linearly in the measured voltage range, indicating the formation of Ohmic contacts. After biofunctionalization, the conductance of the FET channel decreased from its intrinsic value of 25 mS to 2.4 mS. The decrease of the channel conductance after surface biofunctionalization has been commonly observed in other similar studies (Kwon et al., 2012; Mao et al. 2011, 2013). The main reason is that after adding the biomolecules to the conducting FET channel, the local geometric deformation and the number of scattering centers across the InN channel was introduced, thereby decreasing the FET channel conductance. We also performed the solution-gate transistor measurement of the RUM-FET in × 0.01 PBS to obtain the transport properties of the device after the biofunctionalization. The channel current increased from 89 nA to 97 nA, as the solution gating voltage is sweeping from −0.5 V to 0.5 V. The increasing channel current along with the increasing gating voltage indicates that the synthesized InN film was n-type, which is also consistent with the studies using sputtered InN thin film (Saito and Igasaki, 2001). The carrier mobility degradation of the FET channel after biofunctionalization was also clearly observed. From Fig. 4b, it can be seen that the FET transport curve becomes flatter after the biofunctionalization, and the on/off ratio of the device decreases from 1.08 to 1.01. The carrier mobility degradation could be explained by the disordered potential induced by the direct binding of biomolecules (Mao et al. 2010, 2011, 2013).

3.4. Detection of HIV gp41 antibody

The analytical performance of the device was evaluated using HIV-1 envelope gp41 antibody in PBS. The development of rapid and accurate diagnostic tools for POC diagnosis of HIV is of paramount importance for effective control of HIV infections (Davis et al., 2013; May 2017). The HIV-1 envelope gp41 antibody is one the most commonly used HIV markers (Chin et al., 2011). To achieve specific detection of the gp41 antibody, 10 μg mL^{-1} of HIV gp41 antigen was used to bind with the APTMS linkers on the InN surface. The HIV-1 gp41 antibody was diluted

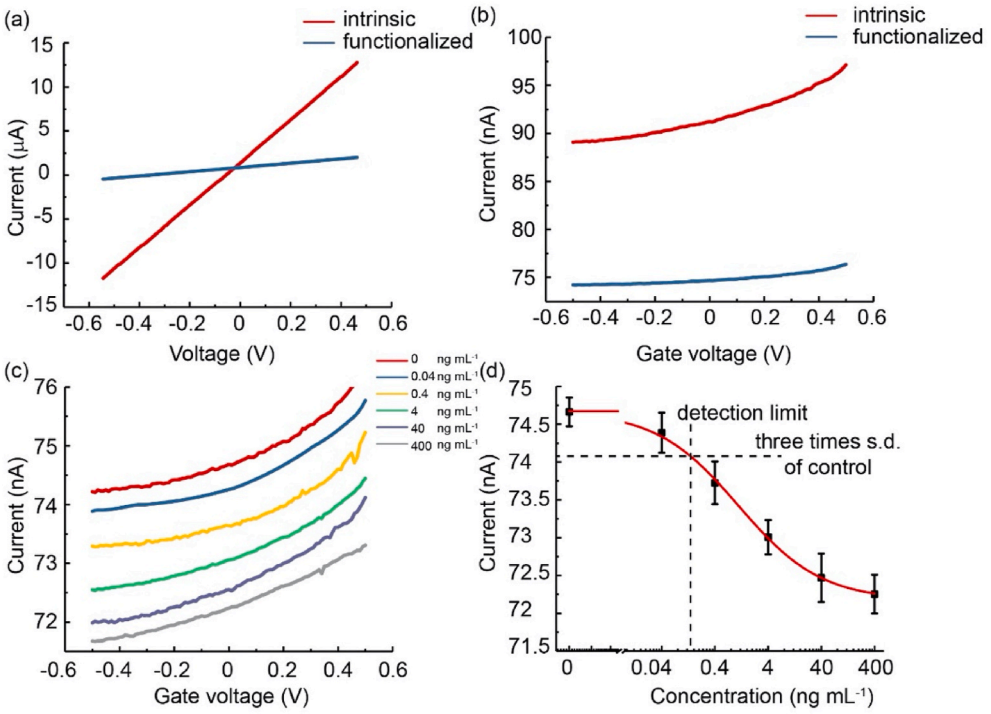

Fig. 6. Electrical characterization of the rolled-up InN FET-type biosensor, and sensing of HIV gp41 antibody in PBS solution. (a) Source-to-drain current measurement results of the device before and after modification with HIV gp41 antigen (10 μg mL^{-1}). (b) Transport measurement results of the device before and after modification with HIV gp41 antigen (10 μg mL^{-1}). (c) Representative transport curves in response to HIV gp41 antibody at increased concentrations. (d) Calibration results of rolled-up InN FET biosensor sensing results of HIV gp41 antibody, with data fitted into an S curve (N = 3).

with 0.01 × PBS solution into different concentrations, and then tested using the developed InN RUM-FET biosensor.

Representative FET curves obtained from the HIV-1 calibration experiments are shown in Fig. 6c. It can be observed that the source-to-drain current decreased with the increasing concentration of the HIV-1 gp41 antibody, which is the typical response of a FET biosensor. The n-type characteristics of the rolled-up InN FET biosensor contributes to the reduced channel conductance with increasing antibody concentration. As the gp41 antibody has a mildly acidic isoelectric point (pI) of ~6.9, it is negatively charged in the 0.01 × PBS solution with the pH value around 7.4 (Gallerano et al., 2015). Therefore, the attachment of a negatively charged molecule to the InN channels is equivalent to a negative potential gating, which leads to a reduced electron density and thus electrical conductivity of the InN channel. The calibration results for detection of gp41 antibody in 0.01 × PBS are shown in Fig. 6d, which was fitted in an S-curve based on the Hill equation. The LOD of the InN RUM-FET biosensor was determined to be 0.1 ng mL^{-1}, which is 20 times lower than that (2 ng mL^{-1}) of the standard ELISA kit. As indicated in the supplementary material, the device variations were mainly induced by the biofunctionalization of InN. By optimizing the biofunctionalization step, we envision that the LOD could be further improved. In our future work, we will also fully characterize the electronic characteristics of the InN microtube FET, which could provide useful guidance on optimizing the FET design for biosensing performance.

Compared to other existing rolled-up microtube biosensors, our device demonstrates the detection of real disease biomarkers with an acceptable LOD. In one of the most similar studies that reported a rolled-up InGaAs/GaAs FET biosensor, only the detection of organic solvents was demonstrated. The detection of clinically relevant biomarkers. such as cells (Bausch et al., 2017; Smith et al., 2011), nucleic acid (Medina-Sánchez et al., 2016), and proteins (Yu et al., 2014), has also been demonstrated using other types of rolled-up microtube-based sensing mechanisms including optical ring resonator (ORR), electrochemical impedance spectroscopy (EIS), and self-propelled micromotor-based sensing. The ORR sensing, though highly sensitive, requires an expensive micro-photoluminescence microscope, making it less practical for use at the point of care (Smith et al., 2011). The rolled-up EIS biosensor shows ultrahigh sensitivity capable of detecting as low as 20 aM of avian influenza virus (Medina-Sánchez et al., 2016). The EIS and FET-based biosensing mechanism both share similar merits such as high sensitivity, microfluidic integration, ease of electrical measurement, and thereby hold great potential for use in clinical diagnosis.

4. Conclusions

In this paper, we presented the development of the microfluidic InN RUM-FET biosensor for label-free detection of HIV antibody. The rolled-up InN microtube was successfully fabricated with a high yield, benefiting from the robust and reliable microfabrication process. The sputtered InN film was characterized using the various characterization tools, demonstrating the successful synthesis of high-quality InN films. The developed InN RUM-FETs, with an external reference electrode, were integrated into microfluidic channels for convenient fluid handling and reduced sample/reagent consumptions. Using HIV envelope gp41 antibody as a model analyte, we achieved a LOD of 01 ng mL^{-1}, which is 20 times lower than that of standard ELISA. Compared to other existing rolled-up microtube biosensors, our device demonstrates the detection of real disease biomarkers with an acceptable LOD. In one of the most similar studies that reported a rolled-up InGaAs/GaAs FET biosensor, only the detection of organic solvents was demonstrated. The detection of clinically relevant biomarkers. such as cells (Bausch et al., 2017; Smith et al., 2011), nucleic acid (Medina-Sánchez et al., 2016), and proteins (Yu et al., 2014), has also been demonstrated using other types of rolled-up microtube-based sensing mechanisms including optical ring resonator (ORR), electrochemical impedance spectroscopy (EIS), and self-propelled micromotor-based sensing. The ORR sensing, though highly sensitive, requires an expensive micro-photoluminescence microscope, making it less practical for use at the point of care (Smith et al., 2011). The rolled-up EIS biosensor shows ultrahigh sensitivity capable of detecting as low as 20 aM of avian influenza virus (Medina-Sánchez et al., 2016). The EIS and FET-based biosensing mechanism both share similar merits such as high sensitivity, microfluidic integration, ease of electrical measurement, and thereby hold great potential for use in

clinical diagnosis.

CRediT authorship contribution statement

Pengfei Song: Conceptualization, Writing – original draft, Writing – review & editing. **Hao Fu:** Validation. **Yongjie Wang:** Validation. **Cheng Chen:** Investigation. **Pengfei Ou:** Investigation. **Roksana Tonny Rashid:** Validation. **Sixuan Duan:** Writing – review & editing. **Jun Song:** Conceptualization. **Zetian Mi:** Conceptualization. **Xinyu Liu:** Conceptualization, Writing – review & editing.

Declaration of competing interest

The authors declare that they have no known competing financial interests or personal relationships that could have appeared to influence the work reported in this paper.

Acknowledgments

This research was supported by Natural Sciences and Engineering Research Council of Canada (NSERC) (grant numbers: STPGP-2014-463182, RGPIN-2017-06374, and RGPAS-2017-507980), and the Canada Foundation for Innovation (grant number: JELF-37812). The financial support from Xi'an Jiaotong – Liverpool University to P. Song is also acknowledged (grant numbers: RDF-18-02-20, KSF-E-39). The authors also acknowledge the financial support from the University of Toronto to X. Liu (through the Percy Hart Edward Professorship) and the Chinese Scholarship Council to P. Song and C. Chen (through CSC scholarships). The authors also acknowledge the financial support from CMC Microsystems for microfabrication.

Appendix A. Supplementary data

Supplementary data to this article can be found online at https://doi.org/10.1016/j.bios.2021.113264.

References

Ang, P.K., Li, A., Jaiswal, M., Wang, Y., Hou, H.W., Thong, J.T., Lim, C.T., Loh, K.P., 2011. Flow sensing of single cell by graphene transistor in a microfluidic channel. Nano Lett. 11 (12), 5240–5246.

Bausch, C.S., Heyn, C., Hansen, W., Wolf, I.M., Diercks, B.-P., Guse, A.H., Blick, R.H., 2017. Ultra-fast cell counters based on microtubular waveguides. Sci. Rep. 7 (1), 1–11.

Bernardi, A., Kiravittaya, S., Rastelli, A., Songmuang, R., Thurmer, D., Benyoucef, M., Schmidt, O., 2008. On-chip Si/SiOx microtube refractometer. Appl. Phys. Lett. 93 (9), 094106.

Chang, Y.-H., Lu, Y.-S., Hong, Y.-L., Gwo, S., Yeh, J.A., 2010. Highly sensitive pH sensing using an indium nitride ion-sensitive field-effect transistor. IEEE Sens. 11 (5), 1157–1161.

Chen, C.-F., Wu, C.-L., Gwo, S., 2006. Organosilane functionalization of InN surface. Appl. Phys. Lett. 89 (25), 252109.

Chin, C.D., Laksanasopin, T., Cheung, Y.K., Steinmiller, D., Linder, V., Parsa, H., Wang, J., Moore, H., Rouse, R., Umviligihozo, G., 2011. Microfluidics-based diagnostics of infectious diseases in the developing world. Nat. Med. 17 (8), 1015.

Cui, X., Kong, Z., Gao, E., Huang, D., Hao, Y., Shen, H., Di, C.-a., Xu, Z., Zheng, J., Zhu, D., 2018. Rolling up transition metal dichalcogenide nanoscrolls via one drop of ethanol. Nat. Commun. 9 (1), 1–7.

Cui, Y., Wei, Q., Park, H., Lieber, C.M., 2001. Nanowire nanosensors for highly sensitive and selective detection of biological and chemical species. Science 293 (5533), 1289–1292.

Dastjerdi, M., Djavid, M., Mi, Z., 2015. An electrically injected rolled-up semiconductor tube laser. Appl. Phys. Lett. 106 (2), 021114.

Davis, D.H., Smith, R., Brown, A., Rice, B., Yin, Z., Delpech, V., 2013. Early diagnosis and treatment of HIV infection: magnitude of benefit on short-term mortality is greatest in older adults. Age Ageing 42 (4), 520–526.

Egunov, A.I., Dou, Z., Karnaushenko, D.D., Hebenstreit, F., Kretschmann, N., Akgün, K., Ziemssen, T., Karnaushenko, D., Medina-Sánchez, M., Schmidt, O.G., 2021. Impedimetric microfluidic sensor-in-a-tube for label-free immune cell analysis. Small 17 (5), 2002549.

Fathil, M., Ghazali, M., Arshad, M.M., Nadzirah, S., Ayub, R., Ruslinda, A., Hashim, U., Abdullah, R., Ong, C., Tamjis, N., 2018. Numerical simulation of different silicon nanowire field-effect transistor channel lengths for biosensing application. In: AIP Conference Proceedings. AIP Publishing LLC, 020007.

Fu, H., Song, P., Wu, Q., Zhao, C., Pan, P., Li, X., Li-Jessen, N.Y., Liu, X., 2019. A paper-based microfluidic platform with shape-memory-polymer-actuated fluid valves for automated multi-step immunoassays. Microsyst. Nanoeng. 5 (1), 1–12.

Gallerano, D., Wollmann, E., Lupinek, C., Schlederer, T., Ebner, D., Harwanegg, C., Niespodziana, K., Schmetterer, K., Pickl, W., Puchhammer-Stöckl, E., 2015. HIV microarray for the mapping and characterization of HIV-specific antibody responses. Lab Chip 15 (6), 1574–1589.

Grimm, D., Bof Bufon, C.C., Deneke, C., Atkinson, P., Thurmer, D.J., Schäffel, F., Gorantla, S., Bachmatiuk, A., Schmidt, O.G., 2013. Rolled-up nanomembranes as compact 3D architectures for field effect transistors and fluidic sensing applications. Nano Lett. 13 (1), 213–218.

Gubbins, P.O., Klepser, M.E., Dering-Anderson, A.M., Bauer, K.A., Darin, K.M., Klepser, S., Matthias, K.R., Scarsi, K., 2014. Point-of-care testing for infectious diseases: opportunities, barriers, and considerations in community pharmacy. Am. Pharm. Assoc. 54 (2), 163–171.

Han, D., Fang, Y., Du, D., Huang, G., Qiu, T., Mei, Y., 2016. Automatic molecular collection and detection by using fuel-powered microengines. Nanoscale 8 (17), 9141–9145.

Hu, N., Sun, M., Lin, X., Gao, C., Zhang, B., Zheng, C., Xie, H., He, Q., 2018. Self-propelled rolled-up polyelectrolyte multilayer microrockets. Adv. Funct. Mater. 28 (25), 1705684.

Huang, G., Bolaños Quiñones, V.A., Ding, F., Kiravittaya, S., Mei, Y., Schmidt, O.G., 2010. Rolled-up optical microcavities with subwavelength wall thicknesses for enhanced liquid sensing applications. ACS Nano 4 (6), 3123–3130.

Jager, E.W., Smela, E., Inganäs, O., 2000. Microfabricating conjugated polymer actuators. Science 290 (5496), 1540–1545.

Karnaushenko, D.D., Karnaushenko, D., Grafe, H.J., Kataev, V., Büchner, B., Schmidt, O. G., 2018. Rolled-up self-assembly of compact magnetic inductors, transformers, and resonators. Adv. Electron. Mater. 4 (11), 1800298.

Kauffman, D.R., Star, A., 2008. Electronically monitoring biological interactions with carbon nanotube field-effect transistors. Chem. Soc. Rev. 37 (6), 1197–1206.

Kwon, O.S., Park, S.J., Hong, J.-Y., Han, A.-R., Lee, J.S., Lee, J.S., Oh, J.H., Jang, J., 2012. Flexible FET-type VEGF aptasensor based on nitrogen-doped graphene converted from conducting polymer. ACS Nano 6 (2), 1486–1493.

Li, F., Mi, Z., 2009. Optically pumped rolled-up InGaAs/GaAs quantum dot microtube lasers. Opt Express 17 (22), 19933–19939.

Li, X., 2011. Self-rolled-up microtube ring resonators: a review of geometrical and resonant properties. Adv. Opt Photon 3 (4), 366–387.

Li, X., Liu, X., 2016. A microfluidic paper-based origami nanobiosensor for label-free, ultrasensitive immunoassays. Adv. Healthcare Mater. 5 (11), 1326–1335.

Li, Y., Hu, P., Feng, L., Du, M., Su, X., Li, Q., Yun, F., 2019. InGaN microtube optical resonator with sub-wavelength wall thickness and its application to refractive index sensing. J. Appl. Phys. 126 (7), 075708.

Lindgren, T., Larsson, M., Lindquist, S.-E., 2002. Photoelectrochemical characterisation of indium nitride and tin nitride in aqueous solution. Sol. Energy Mater. Sol. Cell. 73 (4), 377–389.

Lindgren, T., Torres, G.R., Ederth, J., Karmhag, R., Granqvist, C.-G., Lindquist, S.-E., 2006. DC magnetron reactive sputtered InN thin film electrodes as photoanodes in aqueous solution. A study of as prepared and nitrogen annealed electrodes. Thin Solid Films 510 (1–2), 6–14.

Lu, H., Schaff, W.J., Eastman, L.F., 2004. Surface chemical modification of InN for sensor applications. Appl. Phys. 96 (6), 3577–3579.

Lu, H., Schaff, W.J., Eastman, L.F., Stutz, C., 2003. Surface charge accumulation of InN films grown by molecular-beam epitaxy. Appl. Phys. Lett. 82 (11), 1736–1738.

Mahboob, I., Veal, T.á, McConville, C.á, Lu, H., Schaff, W.á, 2004. Intrinsic electron accumulation at clean InN surfaces. Phys. Rev. Lett. 92 (3), 036804.

Mao, S., Lu, G., Yu, K., Bo, Z., Chen, J., 2010. Specific protein detection using thermally reduced graphene oxide sheet decorated with gold nanoparticle-antibody conjugates. Adv. Mater. 22 (32), 3521–3526.

Mao, S., Yu, K., Chang, J., Steeber, D.A., Ocola, L.E., Chen, J., 2013. Direct growth of vertically-oriented graphene for field-effect transistor biosensor. Sci. Rep. 3 (1), 1–6.

Mao, S., Yu, K., Lu, G., Chen, J., 2011. Highly sensitive protein sensor based on thermally-reduced graphene oxide field-effect transistor. Nano Res. 4 (10), 921.

May, M.T., 2017. Better to know: the importance of early HIV diagnosis. Lancet Publ. Health 2 (1), e6–e7.

Medina-Sánchez, M., Ibarlucea, B., Pérez, N.s., Karnaushenko, D.D., Weiz, S.M., Baraban, L., Cuniberti, G., Schmidt, O.G., 2016. High-performance three-dimensional tubular nanomembrane sensor for DNA detection. Nano Lett. 16 (7), 4288–4296.

Mei, Y., Huang, G., Solovev, A.A., Ureña, E.B., Mönch, I., Ding, F., Reindl, T., Fu, R.K., Chu, P.K., Schmidt, O.G., 2008. Versatile approach for integrative and functionalized tubes by strain engineering of nanomembranes on polymers. Adv. Mater. 20 (21), 4085–4090.

Mei, Y., Thurmer, D.J., Deneke, C., Kiravittaya, S., Chen, Y.-F., Dadgar, A., Bertram, F., Bastek, B., Krost, A., Christen, J.r, 2009. Fabrication, self-assembly, and properties of ultrathin AlN/GaN porous crystalline nanomembranes: tubes, spirals, and curved sheets. ACS Nano 3 (7), 1663–1668.

Mönch, I., Makarov, D., Koseva, R., Baraban, L., Karnaushenko, D., Kaiser, C., Arndt, K.-F., Schmidt, O.G., 2011. Rolled-up magnetic sensor: nanomembrane architecture for in-flow detection of magnetic objects. ACS Nano 5 (9), 7436–7442.

Naoi, H., Muto, D., Hioka, T., Hayakawa, Y., Suzuki, A., Araki, T., Nanishi, Y., 2007. Thermal and chemical stabilities of In-and N-polar InN surfaces. Phys. Status Solidi 244 (6), 1834–1838.

Oseki, M., Okubo, K., Kobayashi, A., Ohta, J., Fujioka, H.J.S.r, 2014. Field-effect transistors based on cubic indium nitride. Sci. Rep. 4 (1), 1–4.

Pant Pai, N., 2007. Oral fluid-based rapid HIV testing: issues, challenges and research directions. Expert Rev. Mol. Diagn. 7 (4), 325–328.
Qin, Z., Peng, R., Baravik, I.K., Liu, X., 2020. Fighting COVID-19: integrated micro- and nanosystems for viral infection diagnostics. Matter 3 (3), 628–651.
Saito, N., Igasaki, Y., 2001. Electrical and optical properties of InN films prepared by reactive sputtering. Appl. Surf. Sci. 169, 349–352.
Shoorideh, K., Chui, C.O., 2014. On the origin of enhanced sensitivity in nanoscale FET-based biosensors. Proc. Natl. Acad. Sci. Unit. States Am. 111 (14), 5111–5116.
Smith, E.J., Schulze, S., Kiravittaya, S., Mei, Y., Sanchez, S., Schmidt, O.G., 2011. Lab-in-a-tube: detection of individual mouse cells for analysis in flexible split-wall microtube resonator sensors. Nano Lett. 11 (10), 4037–4042.
Song, P., Chen, C., Qu, J., Ou, P., Dastjerdi, M., Mi, Z., Song, J., Liu, X., 2018. Rolled-up SiO x/SiN x microtubes with an enhanced quality factor for sensitive solvent sensing. Nanotechnology 29 (41), 415501.
Stern, E., Wagner, R., Sigworth, F.J., Breaker, R., Fahmy, T.M., Reed, M.A., 2007. Importance of the Debye screening length on nanowire field effect transistor sensors. Nano Lett. 7 (11), 3405–3409.
Vickerman, P., Watts, C., Peeling, R., Mabey, D., Alary, M., 2006. Modelling the cost effectiveness of rapid point of care diagnostic tests for the control of HIV and other sexually transmitted infections among female sex workers. Sex. Transm. Infect. 82 (5), 403–412.
Wang, L., Zhou, X., Yang, S., Huang, G., Mei, Y., 2019. 2D-material-integrated whispering-gallery-mode microcavity. Photon. Res. 7 (8), 905–916.
Xu, G., Abbott, J., Qin, L., Yeung, K.Y., Song, Y., Yoon, H., Kong, J., Ham, D., 2014. Electrophoretic and field-effect graphene for all-electrical DNA array technology. Nat. Commun. 5 (1), 1–9.
Xu, W., Qin, Z., Chen, C.-T., Kwag, H.R., Ma, Q., Sarkar, A., Buehler, M.J., Gracias, D.H., 2017. Ultrathin thermoresponsive self-folding 3D graphene. Sci. Adv. 3 (10), e1701084.
Yager, P., Domingo, G.J., Gerdes, J., 2008. Point-of-care diagnostics for global health. Annu. Rev. Biomed. Eng. 10.
Yin, Y., Qiu, T., Ma, L., Lang, X., Zhang, Y., Huang, G., Mei, Y., Schmidt, O.G., 2012. Exploring rolled-up Au–Ag bimetallic microtubes for surface-enhanced Raman scattering sensor. J. Phys. Chem. C 116 (48), 25504–25508.
Yu, X., Arbabi, E., Goddard, L.L., Li, X., Chen, X., 2015. Monolithically integrated self-rolled-up microtube-based vertical coupler for three-dimensional photonic integration. Appl. Phys. Lett. 107 (3), 031102.
Yu, X., Li, Y., Wu, J., Ju, H., 2014. Motor-based autonomous microsensor for motion and counting immunoassay of cancer biomarker. Anal. Chem. 86 (9), 4501–4507.
Zakharchenko, S., Sperling, E., Ionov, L., 2011. Fully biodegradable self-rolled polymer tubes: a candidate for tissue engineering scaffolds. Biomacromolecules 12 (6), 2211–2215.
Zhang, Y., Han, D., Du, D., Huang, G., Qiu, T., Mei, Y., 2015. Rolled-up Ag-SiOx hyperbolic metamaterials for surface-enhanced Raman scattering. Plasmonics 10 (4), 949–954.
Zhao, C., Liu, X., 2016. A portable paper-based microfluidic platform for multiplexed electrochemical detection of human immunodeficiency virus and hepatitis C virus antibodies in serum. Biomicrofluidics 10 (2), 024119.
Zhao, F., Zhan, T., Huang, G., Mei, Y., Hu, X., 2012. Liquid sensing capability of rolled-up tubular optical microcavities: a theoretical study. Lab Chip 12 (19), 3798–3802.
Zhou, X., Tian, Z., Kim, H.J., Wang, Y., Xu, B., Pan, R., Chang, Y.J., Di, Z., Zhou, P., Mei, Y., 2019. Rolling up MoSe2 nanomembranes as a sensitive tubular photodetector. Small 15 (42), 1902528.